Hindawi Publishing Corporation
EURASIP Journal on Wireless Communications and Networking
Volume 2006, Article ID 91329, Pages 1–12
DOI 10.1155/WCN/2006/91329

High-Speed Turbo-TCM-Coded Orthogonal Frequency-Division Multiplexing Ultra-Wideband Systems

Yanxia Wang, Libo Yang, and Lei Wei

School of Electrical Engineering and Computer Science, University of Central Florida, Orlando, FL 32816, USA

Received 30 August 2005; Revised 15 February 2006; Accepted 16 February 2006

One of the UWB proposals in the IEEE P802.15 WPAN project is to use a multiband orthogonal frequency-division multiplexing (OFDM) system and punctured convolutional codes for UWB channels supporting a data rate up to 480 Mbps. In this paper, we improve the proposed system using turbo TCM with QAM constellation for higher data rate transmission. We construct a punctured parity-concatenated trellis codes, in which a TCM code is used as the inner code and a simple parity-check code is employed as the outer code. The result shows that the system can offer a much higher spectral efficiency, for example, 1.2 Gbps, which is 2.5 times higher than the proposed system. We identify several essential requirements to achieve the high rate transmission, for example, frequency and time diversity and multilevel error protection. Results are confirmed by density evolution.

1. INTRODUCTION

In recent years, ultra-wideband (UWB) communications has received great interest from both the academic community and industry. Using extremely wide transmission bandwidths, the UWB signal has the potential for improving the ability to accurately measure position location and range, immunity to significant fading, high multiple-access capability, extremely high data rate at short ranges, and easier material penetrations [1–3]. It is essential for a wireless system to deal with the existence of multiple propagation paths (multipath) exhibiting different delays, which are the result of objects in the environment causing multiple reflections on the way to the receiver. The large bandwidth of UWB waveforms significantly increases the ability of the receiver to resolve the different reflections in the channel. Two basic solutions for inter-symbol interference (ISI) caused by multipath channels are equalization and orthogonal frequency-division multiplexing (OFDM) [4].

OFDM is a promising solution for efficiently capturing multipath energy in highly dispersive UWB channels and delivering high data rate transmission. One of OFDM's successes is its adoption as the standard of choice in wireless personal area networks (WPAN) and wireless local area network (WLAN) systems (e.g., IEEE P802.15-03 [5], IEEE 802.11a, IEEE 802.11g, Hiper-LAN II). Convolutional encoded OFDM has been introduced as the proposed standard to combat flat fading experienced in each subcarrier [6]. The incoming information bits are channel coded prior to serial-to-parallel conversion and carefully interleaved. This procedure splits the information to be transmitted over a large number of subcarriers. At the same time, it provides a link between bits transmitted on those separated subcarriers of the signal spectrum in such a way that information conveyed by faded subcarriers can be reconstructed through the coding link to the information conveyed by well-received subcarriers.

Trellis-coded modulation (TCM), proposed by Ungerboeck [7], is a well-established technique in digital communications for obtaining significant coding gains ($3 \sim 6$ dB), while sacrificing neither data rate nor bandwidth. Recently compound codes have attracted much interest. Examples of such compound codes include turbo TCM (TTCM) [8–10], multilevel codes [11], and parity-concatenated codes [12, 13]. Among the aforementioned compound codes, TTCM is an attractive scheme for higher data rate transmission, since it combines the impressive near Shannon limit error-correcting ability of turbo codes with the high spectral efficiency property of TCM codes. Different schemes using TTCM have been presented in the literature by several authors [8–10].

The basic idea in [8] is to map the encoded bits of a conventional turbo code (possibly after puncturing some of the parity bits to obtain a desired spectral efficiency) to a certain constellation. The decoding is performed by first calculating the log-likelihood ratios of the transmitted systematic

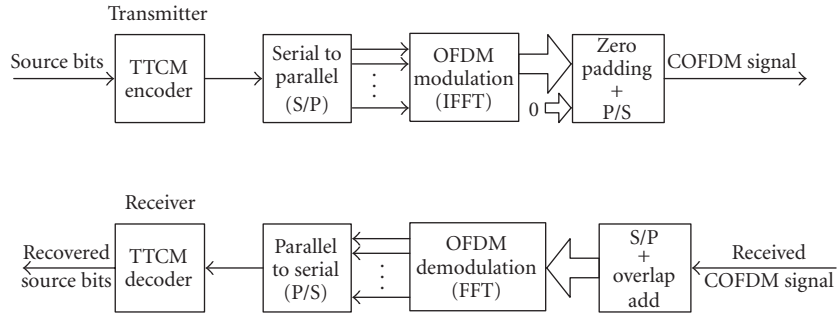

Figure 1: Block diagram of coded OFDM system.

and parity bits, and then using conventional turbo decoding technology. The approach in [9] concatenates two simple trellis codes in parallel. The interleaver before the second trellis encoder operates on groups of information bits. A generalized decoding scheme used for decoding conventional binary turbo codes is used in this case. Benedetto et al. proposed TTCM in [10] where two component convolutional codes are used to produce parity-check bits, with the entire information block and its interleaved version as inputs. The outputs of the two component codes are punctured in such a way that only half of the systematic bits are outputted for the first component code and the other alternative half is outputted by the second component code. Then, the combination of systematic bits, together with the parity check bits from the component codes, is mapped onto a higher constellation. The MAP decoding algorithm is used in this scheme and achieves a performance better than two other schemes [10].

In this paper, we apply a TTCM encoder similar to that in [10] to examine the possible improvement for UWB/OFDM. We found a simple way to construct the encoder, equivalent to describing the turbo code as a simple repetition (i.e., the simplest parity-check code), an interleaver, and TCM, similar to the RA code structure [14]. Then, the bit MAP algorithm is applied in iterative decoding. The code performance is examined when applied to the OFDM systems in the UWB channel environments. Such a system can offer data rates of 640 Mbps via 16-QAM modulation and 1.2 Gbps via 64-QAM modulation. The code performance is confirmed by density evolution.

The paper is organized as follows. Section 2 presents the system description. Section 3 describes the coding and decoding scheme used in the UWB/OFDM system. Section 4 evaluates the code performance through density evolution. Numerical results are given in Section 5, followed by the conclusion section.

2. SIGNAL AND SYSTEM

In this section, we describe the coded OFDM (COFDM) signal and system and the UWB channel model.

2.1. OFDM system

The block diagram of the functions included in the COFDM system is presented in Figure 1. On the transmitter side, source information bits are first encoded and then mapped onto a higher-sized constellation, such as QPSK, 16-QAM, or 64-QAM. Then, the streams of mapped complex numbers are grouped to modulate subcarriers in OFDM frequency band. FFT and inverse FFT (IFFT) are used for a simple implementation [6]. IFFT is performed to construct the so-called "time-domain" OFDM symbols. After the IFFT at the transmitter, a certain length of trailing zeros is padded to avoid interblock interference (IBI). At the receiver side, the reverse-order operations are performed to recover the source information.

The FCC specifies that a system must occupy a minimum of 500 MHz bandwidth in order to be classified as a UWB system. The P802.15-03 project [5] defined a unique numbering system for all channels having a spacing of 528 MHz and lying within the band 3.1–10.6 GHz. According to [15], a 128-point FFT with cyclic prefix length of 60.6 nanoseconds outperforms a 64-point FFT with a prefix length of 54.9 nanoseconds by approximately 0.9 dB. Therefore, we focus on an OFDM system with a 128-point FFT and 528 MHz operating bandwidth. Subcarrier allocation can be found in [5].

We group 100 mapped 16-QAM or 64-QAM complex numbers to modulate 100 data carriers (or data tones) in an OFDM system with a 128-point FFT. Twelve of the subcarriers are dedicated to pilot signals in order to make coherent detection. Ten of the subcarriers are dedicated to guard tones for various purposes, such as relaxing the specifications on the transmitter and receiver filters. In a discrete-time implementation, 128 modulated subcarriers are mapped to the IFFT inputs 1 to 61 and 67 to 127. The rest of the inputs, 62 to 66 and 0, are all set to zero. After the IFFT operation, a length of $D = 32$ trailing zeros is appended to the IFFT output and a guard interval of length 5 is added at the end of the IFFT output to generate an output with the desired length of 165 samples.

Let C_n denote the complex number vector corresponding to subcarrier n of ith OFDM symbol, which includes ith $M \times 1$ information block s_M^i. Then all of the OFDM symbols $\tilde{s}_M^i$ can be constructed using an IFFT through the expression below:

$$\tilde{s}_M^i(t + T_{\mathrm{CP}}) = \begin{cases} \sum_{-N_{\mathrm{ST}}/2}^{N_{\mathrm{ST}}/2} C_n e^{(j2\pi n \Delta_f t)}, & t \in [0, T_{\mathrm{FFT}}], \\ 0, & \text{elsewhere}, \end{cases} \quad (1)$$

where the parameters Δ_f (528 MHz/128 = 4.125 MHz) and N_{ST} are defined as the subcarrier frequency spacing and the number of total subcarriers used, respectively. The resulting waveform has a duration of $T_{FFT} = 1/\Delta_f$ (242.42 nanoseconds). A zero-padding cyclic prefix (T_{CP} = 60.61 nanoseconds) is used in OFDM to mitigate the effect of multipath. A guard interval (T_{GI} = 9.47 nanoseconds) ensures that only a single RF transmitter and RF receiver chain is needed for all channel environments and data rates and there is sufficient time for the transmitter and receiver to switch if used in multiband OFDM [15]. T_{FFT}, T_{CP}, and T_{GI} make up the OFDM symbol period T_{sys}, which is 312.5 nanoseconds in this case.

2.2. UWB channel model

Many UWB indoor propagation models have been proposed [16, 17],The IEEE 802.15.3a Study Group selected the model in [17], properly parameterized for the best fit to the certain channel characteristics. There are two basic techniques for the UWB channel sounding—frequency-domain sounding technique and time-domain sounding technique. We use a frequency-domain autoregressive (AR) model [3] since it has far fewer parameters than the time-domain method and allows simple simulation of a UWB channel. As a result, the simulation model can be constructed and the simulation can be performed easily. The frequency response of a UWB channel at each point $H(f_n)$ is modelled by an AR process:

$$H(f_n, x) - \sum_{i=1}^{p} b_i H(f_{n-i}, x) = V(f_n), \tag{2}$$

where $H(f_n, x)$ is the nth sample of the complex frequency response at location x, $V(f_n)$ is complex white noise, the complex constants b_i are the parameters of the model, and p is the order of the model. Based on the frequency-domain measurements in the 4.3 GHz to 5.6 GHz frequency band, a second-order ($p = 2$) AR model is reported to be sufficient for characterization of the UWB indoor channel [3]. For a UWB model realization with the TR separation of LOS 10 m, the estimated complex constants b_i could be

$$\begin{aligned} b_1 &= -1.6524 + 0.8088i, \\ b_2 &= 0.5463 + 0.7381i. \end{aligned} \tag{3}$$

The detailed parameters description can be found in [3].

The OFDM symbol blocks experience IBI when propagating through the UWB channels because the underlying channel's impulse response combines contributions from more than one transmitted block at the receiver. To account for IBI, OFDM systems rely on the so-called cyclic prefix (CP), which consists of redundant symbols replicated at the beginning of each transmitted block, or zero-padding (ZP), which are trailing zeros padded at the end of each transmitted block. To eliminate IBI, the redundant part of each block is chosen greater than the channel length and is discarded at the receiver in a fashion identical to that used in the overlap-save (OLS, for CP) or overlap-add (OLA, for ZP) method of block convolution. That means by inserting the redundant part in the form of CP or ZP, we are able to achieve IBI free reception. Furthermore, when it comes to equalization, such redundancy pays off. Each truncated block at the receiver end is FFT processed—an operation converting the frequency-selective channel into parallel flat-faded independent subchannels—each corresponding to a different subcarrier. Unless zero, flat fades are removed by dividing each subchannel's output with channel transfer function at the corresponding subcarrier. At the expense of bandwidth overexpansion, coded OFDM ameliorates performance losses incurred by channels having nulls on the transmitted subcarriers [18]. CP and ZP methods are equivalent and rely implicitly on the well-known OLS method as opposed to OLA. In the rest of this section, we will focus on IBI removal and postequalization of the Zero padded OFDM system over the UWB channel.

OFDM signal block propagation through UWB channels can be modeled as an FIR filter with the channel impulse response column vector $h = [h_0 h_1 \cdots h_{M-1}]^T$ and additive white Gaussian noise (AWGN) $\tilde{n}_n(i)$ of variance δ_n^2 [18]. Let $\mathbf{F}_M$ denote the FFT matrix with (m,k)th entry $e^{-j2\pi mk/M}/\sqrt{M}$. Then, the IFFT matrix can be denoted as $\mathbf{F}_M^{-1} = \mathbf{F}_M^H$ with (m,k)th entry $e^{j2\pi mk/M}/\sqrt{M}$ to yield the so-called time-domain block vector $\tilde{s}_M^i = \mathbf{F}_M^H s_M^i$, where $(\cdot)^H$ denotes conjugate transposition. If we denote the signal vectors s_M^i and $\tilde{s}_M^i$ as $[s_M^i(0) s_M^i(1) \cdots s_M^i(M-1)]^T$ and $[\tilde{s}_M^i(0) \tilde{s}_M^i(1) \cdots \tilde{s}_M^i(M-1)]^T$, respectively, then padding D zeros onto vector $\tilde{s}_M^i$ is equivalent to extend $M \times M$ matrix $\mathbf{F}_M^H$ to $P \times M$ matrix $\mathbf{F}_{zp} = [\mathbf{F}_M \mathbf{0}]^H$ based upon the relationship between $\tilde{s}_M^i$ and s_M^i. The resultant redundant block $\tilde{s}_{zp}^i$ will have $P = M + D$ samples, which can be denoted as $\tilde{s}_{zp}^i = [\tilde{s}_M^i(0) \tilde{s}_M^i(1) \cdots \tilde{s}_M^i(M-1) 0 \cdots 0]^T = \mathbf{F}_{zp} s_M^i$.In practice, we select $M > D > L$, where L is the channel order (i.e., $h_i = 0$, for all $i > L$). Then, the expression of the ith received symbol block is given by

$$\tilde{x}_{zp}^{\,i} = \mathbf{H}\mathbf{F}_{zp} s_M^i + \mathbf{H}_{IBI}\mathbf{F}_{zp} s_M^{i-1} + \tilde{n}_P^{\,i}, \tag{4}$$

where $\mathbf{H}$ is the $P \times P$ lower triangular Toeplitz filtering matrix and $\mathbf{H}_{IBI}$ is the $P \times P$ upper triangular Toeplitz filtering matrix as follows [19]:

$$H = \begin{pmatrix} h_0 & 0 & \cdots & 0 & 0 \\ h_1 & h_0 & \cdots & 0 & 0 \\ \vdots & & & & \\ h_L & h_{L-1} & \cdots & 0 & 0 \\ 0 & h_L & \cdots & 0 & 0 \\ \vdots & & & & \\ 0 & 0 & \cdots & h_0 & 0 \\ 0 & 0 & \cdots & h_1 & h_0 \end{pmatrix}_{P \times P}, \tag{5}$$

$$\mathbf{H}_{\mathrm{IBI}} = \begin{pmatrix} 0 & \cdots & 0 & h_L & \cdots & h_1 \\ 0 & \cdots & 0 & 0 & \cdots & h_2 \\ \vdots & & & & & \\ 0 & \cdots & 0 & 0 & \cdots & h_L \\ 0 & \cdots & 0 & 0 & \cdots & 0 \\ \vdots & & & & & \\ 0 & \cdots & 0 & 0 & \cdots & 0 \end{pmatrix}_{P\times P}. \tag{5}$$

The IBI in this case is eliminated due to the all-zero $D \times M$ matrix $\mathbf{0}$ in $\mathbf{F}_{\mathrm{zp}}$ which causes $\mathbf{H}_{\mathrm{IBI}}\mathbf{F}_{\mathrm{zp}} = 0$. $\widetilde{n}^{\,i}_{P}$ denotes the AWGN vector.

We partition $\mathbf{H}$ into two parts: $\mathbf{H} = [\mathbf{H}_0, \mathbf{H}_{\mathrm{zp}}]$, where $\mathbf{H}_0$ represents its first M columns and $\mathbf{H}_{\mathrm{zp}}$ its last D columns. Then, the received $P \times 1$ vector becomes

$$\widetilde{x}^{\,i}_{\mathrm{zp}} = \mathbf{H}\mathbf{F}_{\mathrm{zp}}s^i_M + \widetilde{n}^{\,i}_{P} = \mathbf{H}_0\mathbf{F}^H_M s^i_M + \widetilde{n}^{\,i}_{P} \tag{6}$$

since last D rows of $\mathbf{F}_{\mathrm{zp}}$ are all zeros. We then split the signal part in $\widetilde{x}^{\,i}_{\mathrm{zp}}$ in (6) into its upper $M \times 1$ part $\widetilde{x}^{\,i}_{u} = \mathbf{H}_u\widetilde{s}^{\,i}_M$ and its lower $D\times 1$ part $\widetilde{x}^{\,i}_{l} = \mathbf{H}_l\widetilde{s}^{\,i}_M$, where $\mathbf{H}_u$ (or $\mathbf{H}_l$) denotes the corresponding $M \times M$ (or $D \times M$) partition of $\mathbf{H}_0$ as follows:

$$\mathbf{H}_u = \begin{pmatrix} h_0 & 0 & \cdots & 0 & 0 \\ h_1 & h_0 & \cdots & 0 & 0 \\ \vdots & & & & \\ 0 & 0 & \cdots & h_0 & 0 \\ 0 & 0 & \cdots & h_1 & h_0 \end{pmatrix}_{M\times M},$$

$$\mathbf{H}_l = \begin{pmatrix} 0 & \cdots & 0 & h_L & \cdots & h_1 \\ 0 & \cdots & 0 & 0 & \cdots & h_2 \\ \vdots & & & & & \\ 0 & \cdots & 0 & 0 & \cdots & h_L \\ 0 & \cdots & 0 & 0 & \cdots & 0 \\ \vdots & & & & & \\ 0 & \cdots & 0 & 0 & \cdots & 0 \end{pmatrix}_{D\times M}. \tag{7}$$

Padding $M - D$ zeros in $\widetilde{x}^{\,i}_{l}$ and adding the resulting vector to $\widetilde{x}^{\,i}_{u}$, we get

$$\begin{aligned} \widetilde{x}^{\,i}_{M} &= \widetilde{x}^{\,i}_{u} + \begin{bmatrix} \widetilde{x}^{\,i}_{l} \\ \mathbf{0}_{(M-D)\times 1} \end{bmatrix} \\ &= \left(\mathbf{H}_u + \begin{bmatrix} \mathbf{H}_l \\ \mathbf{0}_{(M-D)\times M} \end{bmatrix}\right)\widetilde{s}^{\,i}_M \\ &= \mathbf{C}_M(h)\widetilde{s}^{\,i}_M, \end{aligned} \tag{8}$$

where $\mathbf{C}_M(h)$ is an $M \times M$ circulant matrix as follow:

$$\mathbf{C}_M(h) = \begin{pmatrix} h_0 & 0 & \cdots & h_L & \cdots & h_1 \\ h_1 & h_0 & \cdots & 0 & \cdots & h_2 \\ \vdots & & & & & \\ h_L & h_{L-1} & \cdots & 0 & \cdots & 0 \\ \vdots & & & & & \\ 0 & 0 & \cdots & h_L & \cdots & h_0 \end{pmatrix}_{M\times M}. \tag{9}$$

The noise will be slightly colored due to overlapping and addition (OLA) operation. Then, using FFT to perform demodulation, the received signal in the frequency domain is given by

$$\begin{aligned} X^i_M &= \mathbf{F}_M\mathbf{C}_M(h)\mathbf{F}^H_M s^i_M + \mathbf{F}_M\widetilde{n}^{\,i}_M \\ &= \mathrm{diag}\,(H_0 \cdots H_{M-1})s^i_M + \mathbf{F}_M\widetilde{n}^{\,i}_M \\ &= \mathbf{D}_M(\widetilde{h}_M)s^i_M + \mathbf{n}^i_M, \end{aligned} \tag{10}$$

where $\widetilde{h}_M = [H_0 \cdots H_{M-1}]^T = \sqrt{M}\mathbf{F}_M h$, with $H_k = H(2\pi k/M) = \Sigma_{l=0}^{L} h_l e^{-j2\pi kl/M}$ denoting the channel transfer function on the kth subcarrier, $\mathbf{D}_M(\widetilde{h}_M)$ standing for the $M \times M$ diagonal matrix with $\widetilde{h}_M$ on its diagonal.

3. CODING AND DECODING

3.1. A simplified TTCM coding scheme

The TTCM was proposed by Benedetto et al. in [10]. Each of two component encoders has rate $b/(b + 1)$ (where b is even), but only $b/2$ alternative systematic bits are selected to combine with the corresponding parity-check bit as the outputs for each constitutent encoder. The systematic bits for the second constitutent code are those systematic bits which are punctured in the first encoder. Two bit interleaves are involved in this TTCM encoder. The first interleaver permutes the bits selected by the first encoder and the second interleaves those bits punctured by the first encoder. For M-QAM, there are $2^{1+b/2}$ levels in both I and Q channels, therefore achieving a throughput of b bps/Hz. One of the prototype of the 16-QAM TTCM is illustrated in Figure 2

A simple method can be used to describe the same code in Figure 3. This is equivalent to describing the turbo codes as a repeater (that is the simplest parity-check code), an interleaver, and one component code [14]. Two bit streams (u_1 and u_2) are provided at the input of the TCM encoder—one is the original source information bit stream (u_1), and the other (u_2) is the interleaved version corresponding to the parity checks of the first one. TCM encoder has rate of 2/2, which combines only the original systematic bit (from u_1 stream) and the parity-check bit as the encoder outputs. Then, two consecutive clock cycle outputs (or two outputs after further interleaving) are mapped onto 16-QAM constellation—one for the in-phase component and the other for the quadrature component. If we make the interleaving size of the interleaver before the TCM encoder to

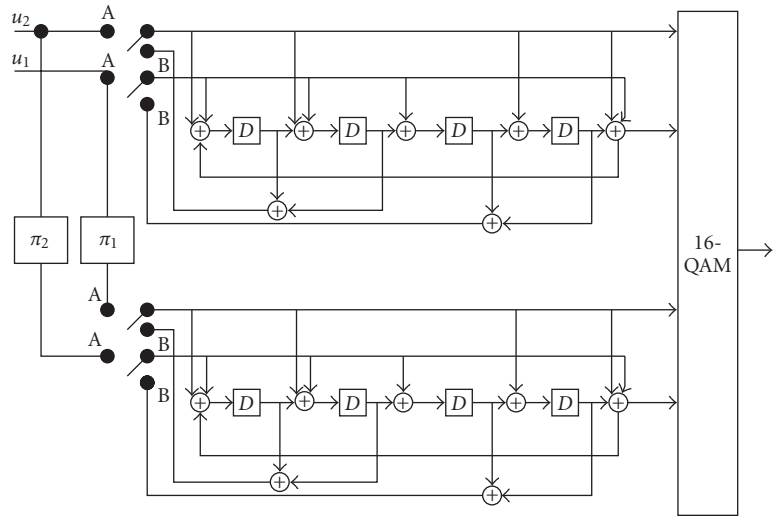

Figure 2: Parallel concatenated trellis-coded modulation,16-QAM.

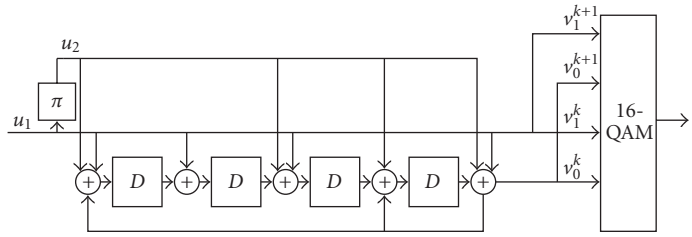

Figure 3: Parity-concantenated TCM encoder,16-QAM.

be half of the information block size, the function of this concatenated structure is exactly the same as that of TTCM.

Figure 4 illustrates the equivalence between TTCM and parity-concatenated TCM. Figure 4(a) is the 16-QAM block diagram of TTCM encoder with short block inputs $\mathbf{u}_1 = u_1^3u_1^2u_1^1u_1^0$ and $\mathbf{u}_2 = u_2^3u_2^2u_2^1u_2^0$, whereas u_1^0 and u_2^0 are the LSBs and u_1^3 and u_2^3 are the MSBs. Assume after interleaving, two input sequences to the second constituent encoder are $u_2^1u_2^0u_2^3u_2^2$ and $u_1^2u_1^0u_1^1u_1^3$, then 4 coded output sequences would be $u_1^3u_1^2u_1^1u_1^0$, $v_1^3v_1^2v_1^1v_1^0$, $u_2^1u_2^0u_2^3u_2^2$, and $v_2^3v_2^2v_2^1v_2^0$. The similar coding results can be obtained through the encoder in Figure 4(b) with only a difference in the partial parity-check bits. The merge from encoder of Figure 4(b) to that of Figure 4(c) is straight forward when we set the interleaver size and pattern as shown in Figure 4(c).

Figure 5 describes the simplified encoder for 64-QAM modulation. There are 4 information streams (u_1, u_2, u_3, and u_4) into the encoder. Among those four information streams, two streams (u_3 and u_4) are the interleaved versions of the original two source streams (u_1 and u_2), respectively. Again, two consecutive clock cycle outputs are mapped onto 64-QAM constellation via Gray mapping.

There are three advantages for such a modification. (a) We consider fewer interleavers: only one interleaver for the 16-QAM case (instead of 2) and 2 interleavers for 64-QAM case (instead of 4). (b) We save one constituent encoder. (c) It is easy to extend this to parity-concatenated codes. That is, we simply replace the repeater with a parity-check code.

When this coding scheme is applied to the OFDM system over the UWB channel, the coded bit stream is interleaved prior to modulation in order to provide robustness against burst errors. The bit interleaving operation is performed in two stages: symbol interleaving followed by OFDM tone interleaving. The symbol interleaver permutes the bits across OFDM symbols to exploit frequency diversity across subbands, while the tone interleaver permutes the bits across the data tones within an OFDM symbol to exploit frequency diversity across tones and provide robustness against narrowband interference.

We constrain our symbol interleaver to a regular block interleaver of *size* $N_P \times$ *number* of encoder output bits, where N_P is the input information packet length and the number of encoder output bits is 2 for 16-QAM and 4 for 64-QAM. The coded bits are read in columnwise and read out rowwise. The output of the symbol block interleaver is then passed through a tone block interleaver of *size* $N_{\mathrm{OFDM}} \times$ *tone* numbers in one OFDM symbol, where N_{OFDM} is the OFDM symbol numbers for one packet and the tone number is 100 for the considered OFDM system. Still the coded bits are read in columnwise and read out rowwise.

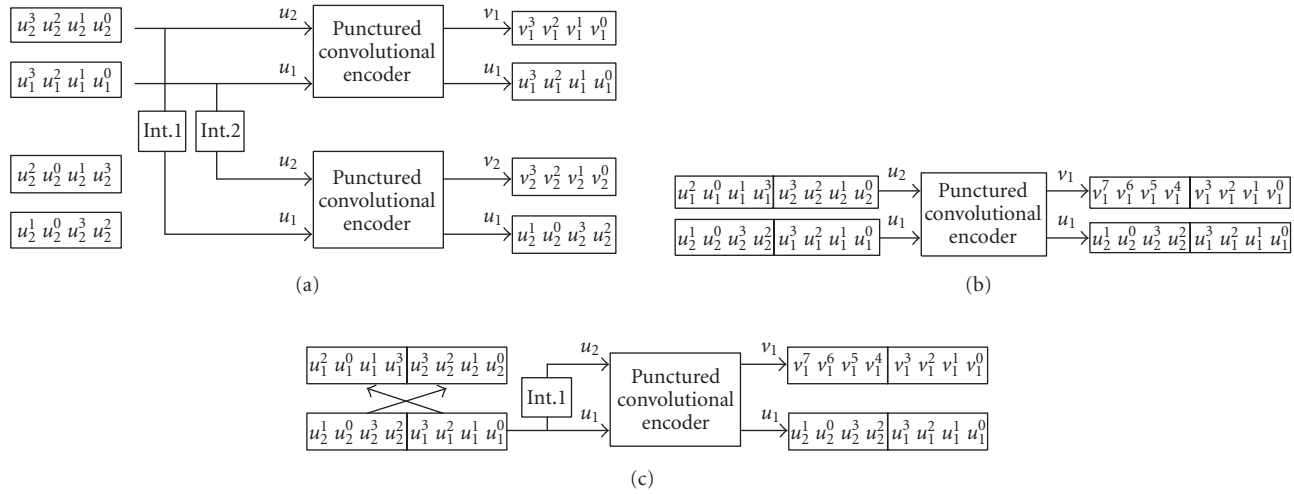

Figure 4: Expansion from Benedetto's TTCM to parity-concatenated TCM.

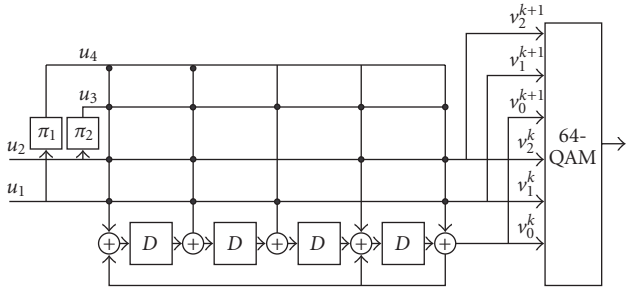

Figure 5: Parity-concatented TCM encoder, 64-QAM.

3.2. Bit iterative MAP decoder

The MAP (maximum a posteriori probability) algorithm in iterative decoding calculates the logarithm of likelihood ratio (LLR), $\Lambda(u_b)$, associated with each decoded bit u_b at time k through (11) [20]:

$$\Lambda(u_b) = \log \frac{P_r\{u_b = 1 \mid \text{observation}\}}{P_r\{u_b = 0 \mid \text{observation}\}}, \tag{11}$$

where $P_r\{u_b = i/\text{observation}\}$, $i = 0, 1$, is the *a posteriori probability* (APP) of the data bit u_b. The APP of a decoded data bit u_b can be derived from the joint probability $\lambda_k^i(m)$ defined by

$$\lambda_k^i(S_k) = P_r\{u_b = i, S_k \mid \mathbf{y}_k\}, \tag{12}$$

where S_k represents the encoder state at time k and $\mathbf{y}_k$ is the received channel symbol. Thus, the APP of a decoded data bit u_b is equal to

$$P_r\{u_b = i \mid \mathbf{y}_k\} = \sum_{S_k} \lambda_k^i(S_k), \quad i = 0, 1. \tag{13}$$

From relations (11) and (13), the LLR $\Lambda(u_b)$ associated with a decoded bit u_b can be written as

$$\Lambda(u_b) = \log \frac{\sum_{S_k} \lambda_k^1(S_k)}{\sum_{S_k} \lambda_k^0(S_k)}. \tag{14}$$

Finally the decoder can make a decision by comparing $\Lambda(u_b)$ to a threshold equal to zero:

$$\begin{aligned} \widetilde{u}_b &= 1 \quad \text{if } \Lambda(u_b) > 0, \\ \widetilde{u}_b &= 0 \quad \text{if } \Lambda(u_b) < 0. \end{aligned} \tag{15}$$

The joint probability $\lambda_k^i(S_k)$ can be rewritten using Bayes rule:

$$\begin{aligned} \lambda_k^i(S_k) &= \frac{P_r\{u_b = i, S_k, \mathbf{y}_1^k, \mathbf{y}_{k+1}^N\}}{P_r\{\mathbf{y}_1^k, \mathbf{y}_{k+1}^N\}} \\ &= \frac{P_r\{u_b = i, S_k, \mathbf{y}_1^k\}}{P_r\{\mathbf{y}_1^k\}} \cdot \\ &\quad \frac{P_r\{\mathbf{y}_{k+1}^N \mid u_b = i, S_k, \mathbf{y}_1^k\}}{P_r\{\mathbf{y}_{k+1}^N \mid \mathbf{y}_1^k\}} \end{aligned} \tag{16}$$

in which we assume the information symbol sequence $\{\mathbf{u}_k\}$ is made up of N independent input symbols $\mathbf{u}_k$ with K input bits (i.e., $u_b, b = 1, \ldots, K$) in each $\mathbf{u}_k$ and take into account that events after time k are not influenced by observations $\mathbf{y}_1^k$ and symbol $\mathbf{u}_k$ if encoder state S_k is known. For easy computation of the probability $\lambda_k^i(S_k)$, probability functions $\alpha_k(S_k)$, $\beta_k(S_k)$, and $\gamma_i(\mathbf{y}_k, S_{k-1}, S_k)$ are introduced as follows [21]:

$$\begin{aligned} \alpha_k(S_k) &= \frac{P_r\{u_b = i, S_k, \mathbf{y}_1^k\} P_r\{u_b = i, S_k \mid \mathbf{y}_1^k\}}{P_r\{\mathbf{y}_1^k\}}, \\ \beta_k(S_k) &= \frac{P_r\{\mathbf{y}_{k+1}^N \mid S_k\}}{P_r\{\mathbf{y}_{k+1}^N \mid \mathbf{y}_1^k\}}, \\ \gamma_i(\mathbf{y}_k, S_{k-1}, S_k) &= P_r\{u_b = i, \mathbf{y}_1^k, S_k \mid S_{k-1}\}. \end{aligned} \tag{17}$$

Then $\lambda_k^i(S_k)$ can be simplified as

$$\lambda_k^i(S_k) = \alpha_k(S_k)\beta_k(S_k). \tag{18}$$

The probabilities $\alpha_k(S_k)$ and $\beta_k(S_k)$ can be recursively calculated from probability $\gamma_i(\mathbf{y}_k, S_{k-1}, S_k)$ through

$$\alpha_k(S_k) = \frac{\sum_{S_{k-1}} \sum_{j=0}^{1} \gamma_i(\mathbf{y}_k, S_{k-1}, S_k)\alpha_{k-1}^j(S_{k-1})}{\sum_{S_k} \sum_{S_{k-1}} \sum_{i=0}^{1} \sum\nolimits_{j=0}^{1} \gamma_i(\mathbf{y}_k, S_{k-1}, S_k)\alpha_{k-1}^j(S_{k-1})},$$

$$\beta_k(S_k) = \frac{\sum_{S_{k-1}} \sum_{j=0}^{1} \gamma_i(\mathbf{y}_{k+1}, S_k, S_{k+1})\beta_{k+1}^j(S_{k+1})}{\sum_{S_{k+1}} \sum_{S_k} \sum_{i=0}^{1} \sum_{j=0}^{1} \gamma_i(\mathbf{y}_{k+1}, S_k, S_{k+1})\alpha_k^j(S_k)}, \tag{19}$$

and $\gamma_i(\mathbf{y}_k, S_{k-1}, S_k)$ can be determined from transition probabilities of the encoder trellis and the channel, which is given by

$$\begin{aligned}\gamma_i(\mathbf{y}_k, S_{k-1}, S_k) &= p(\mathbf{y}_k \mid u_b = i, S_{k-1}, S_k) \\ &\quad \times q(u_b = i \mid S_{k-1}, S_k) \times \\ &\quad \pi(S_k \mid S_{k-1})\end{aligned} \tag{20}$$

$p(\cdot \mid \cdot)$ is the channel transition probability, $q(\cdot \mid \cdot)$ is either 1 or 0 depending on whether the ith bit is associated with transition from S_{k-1} to S_k or not, and $\pi(\cdot \mid \cdot)$ is the state transition probability that uses the extrinsic information of information $\mathbf{u}_k$.

Using LLR $\Lambda(u_b)$ definition (Figure 10) and relations among $\lambda_k^i, \alpha_k, \beta_k$, and γ_i we obtain

$$\Lambda(u_b) = \log \frac{\sum_{S_k} \sum_{S_{k-1}} \gamma_1(\mathbf{y}_k, S_{k-1}, S_k)\alpha_{k-1}(S_{k-1})\beta_k(S_k)}{\sum_{S_k} \sum_{S_{k-1}} \gamma_0(\mathbf{y}_k, S_{k-1}, S_k)\alpha_{k-1}(S_{k-1})\beta_k(S_k)}. \tag{21}$$

It was proven in [20] that the LLR $\Lambda(u_b)$ associated with each decoded bit u_b is the sum of the LLR of u_b at the decoder input and of another information called extrinsic information generated by the decoder.

Divsalar and Pollara [22] described an iterative decoding scheme for q parallel concatenated convolutional codes based on approximating the optimum bit decision rule by considering the combination of interleaver and the trellis encoder as a block encoder. The scheme is based on solving a set of nonlinear equations given by ($q = 2$ is used here to illustrate the concept [10, 22])

$$\begin{aligned}\hat{L}_{1b} &= \log \frac{\sum_{\mathbf{u}:u_b=1} P(\mathbf{y}_1 \mid \mathbf{u}) \prod_{j\neq b} e^{u_j \hat{L}_{2j}}}{\sum_{\mathbf{u}:u_b=0} P(\mathbf{y}_1 \mid \mathbf{u}) \prod_{j\neq b} e^{u_j \hat{L}_{2j}}}, \\ \hat{L}_{2b} &= \log \frac{\sum_{\mathbf{u}:u_b=1} P(\mathbf{y}_2 \mid \mathbf{u}) \prod_{j\neq b} e^{u_j \hat{L}_{1j}}}{\sum_{\mathbf{u}:u_b=0} P(\mathbf{y}_2 \mid \mathbf{u}) \prod_{j\neq b} e^{u_j \hat{L}_{1j}}}\end{aligned} \tag{22}$$

for $b = 1, 2, \ldots, K$ representing b input bits per constituent encoder, where $\hat{L}_{1j}$ are the extrinsic information and $\mathbf{y}_q$ are the received observation vectors corresponding to the qth trellis code. The final decision is then based on $L_b = \hat{L}_{1b} + \hat{L}_{2b}$, which passed through a hard limiter with zero threshold.

The above set of nonlinear equations is derived from the optimum bit decision rule

$$L_b = \log \frac{\sum_{\mathbf{u}:u_b=1} P(\mathbf{y}_1 \mid \mathbf{u})P(\mathbf{y}_2 \mid \mathbf{u})}{\sum_{\mathbf{u}:u_b=0} P(\mathbf{y}_1 \mid \mathbf{u})P(\mathbf{y}_2 \mid \mathbf{u})} \tag{23}$$

using the following approximation:

$$P(\mathbf{u} \mid \mathbf{y}_1) \approx \prod_{b=1}^{N} \frac{e^{u_b \hat{L}_{1b}}}{1 + e^{\hat{L}_{1b}}}, \qquad P(\mathbf{u} \mid \mathbf{y}_2) \approx \prod_{b=1}^{N} \frac{e^{u_b \hat{L}_{2b}}}{1 + e^{\hat{L}_{2b}}}. \tag{24}$$

The nonlinear equations in (23) can be solved by using an iterative procedure

$$\hat{L}_{1b}^{(m+1)} = \log \frac{\sum_{\mathbf{u}:u_b=1} P(\mathbf{y}_1 \mid \mathbf{u}) \prod_{j\neq b} e^{u_j \hat{L}_{2j}^{(m)}}}{\sum_{\mathbf{u}:u_b=0} P(\mathbf{y}_1 \mid \mathbf{u}) \prod_{j\neq b} e^{u_j \hat{L}_{2j}^{(m)}}} \tag{25}$$

on m for $b = 1, 2, \ldots, K$. Similar recursions hold for $\hat{L}_{2b}^{(m+1)}$. The recursion starts with the initial condition $\hat{L}_1^{(0)} = \hat{L}_2^{(0)} = 0$. The LLR of a symbol $\mathbf{u}$ given the observation $\mathbf{y}$ is calculated first using the symbol MAP algorithm

$$\lambda(\mathbf{u}) = \log \frac{P(\mathbf{u} \mid \mathbf{y})}{P(\mathbf{0} \mid \mathbf{y})}, \tag{26}$$

where $\mathbf{0}$ corresponds to the all-zero symbol. The symbol MAP algorithm [21] can be used to calculate (26), as shown in Figure 6 [10]. Then the LLR of the bth bit within the symbol can be obtained by

$$L_b = \log \frac{\sum_{\mathbf{u}:u_b=1} e^{\lambda(\mathbf{u})}}{\sum_{\mathbf{u}:u_b=0} e^{\lambda(\mathbf{u})}}. \tag{27}$$

The symbol a priori probabilities needed in the symbol MAP algorithm, which is used in branch transition probability calculation, can be obtained by

$$P(\mathbf{u}) = \prod_{b=1}^{K} \frac{e^{u_b \hat{L}_b}}{1 + e^{\hat{L}_b}} \tag{28}$$

with the assumption that the extrinsic bit reliabilities coming from the other decoder are independent.

In our case, we apply the turbo iterative MAP decoding scheme in [10, 20, 21], and make certain modifications to fit our concatenated encoder structure. For example, we only need one bit MAP decoder instead of two as in [10] for iterative decoding, since the outer parity-check encoders can be viewed as repeaters. So, the corresponding outer decoders only exchange extrinsic information between repeated bit streams. The decoder structure is depicted in Figure 7.

The bit MAP decoder computes the *a posteriori probabilities* $P(u_b \mid \mathbf{y}, \tilde{\mathbf{u}})$ ($\mathbf{y}$ is the received channel symbol and $\tilde{\mathbf{u}}$ is the result from previous iteration), or equivalently the log-likelihood ratio $\Lambda(u_b) = \log(P(u_b = 1 \mid \mathbf{y}, \tilde{\mathbf{u}})/P(u_b = 0 \mid \mathbf{y}, \tilde{\mathbf{u}}))$. Then, the extrinsic information $L_e(u_b)_{\text{out}}$ is extracted

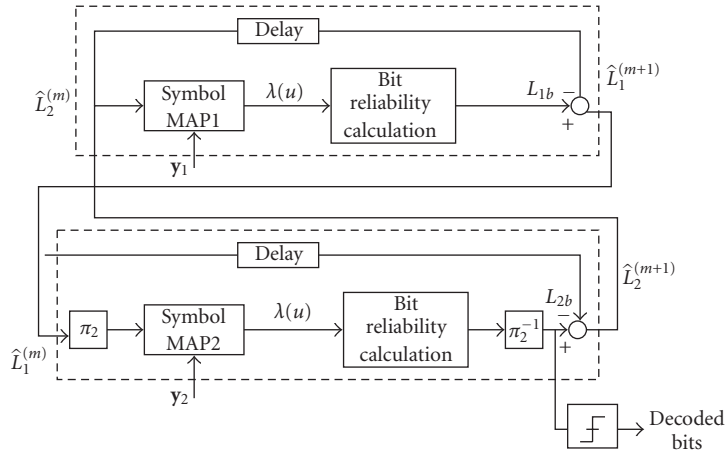

Figure 6: Iterative(trubo)decoder structure for two trellis codes.

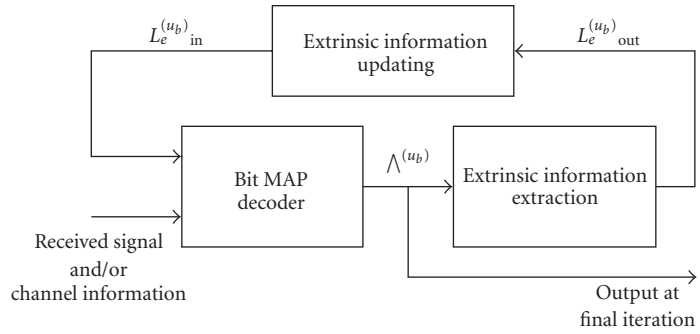

Figure 7: Block diagram of the iterative decoder.

from $L_e(u_b)_{\text{out}} = \Lambda(u_b) - L_c(u_b) - L_e(u_b)_{\text{in}}$ to avoid information being used repeatedly. It will be supplied to the parity-check decoder. The outer parity-check decoder updates the $L_e(u_b)_{\text{out}}$ into $L_e(u_b)_{\text{in}}$ according to parity-check constraints between information bits and supplies it to the bit MAP decoder for the next iteration. $L_e(u_b)_{\text{in}}$ is the extrinsic information, which is used as a priori probability for branch metric computation in MAP decoding process. $L_c(u_b)$ is the channel reliability for each u_b.

Since half of the systematic bits from the inner TCM encoder are punctured, it seems that we can only get channel transition probability for the remaining half of the information bits and parity-check bits. However, the punctured information bits are the parity checks of those systematic bits at the encoder outputs except they are interleaved. So we can always find the channel transition probability for the punctured information bits through the unpunctured part. The extrinsic information value associated with $\pi(\cdot/\cdot)$ in (20) is given as the logarithm format:

$$L_e(u_b) = \log \frac{P(u_b = 1)}{P(u_b = 0)}. \tag{29}$$

If $q(u_b = 1/S_{k-1}, S_k) = 1$, then

$$\pi(S_k/S_{k-1}) = \frac{e^{L_e(u_b)}}{1 + e^{L_e(u_b)}}, \tag{30}$$

otherwise

$$\pi(S_k/S_{k-1}) = \frac{1}{1 + e^{L_e(u_b)}}. \tag{31}$$

4. DENSITY EVOLUTION FOR TTCM

Convergence analysis of iterative decoding algorithms is often used to predict code performance and to provide insight into the encoder structure. One of the methods—extrinsic information transfer (EXIT) method—has been widely used in particular [23–25]. The EXIT chart is a tool for studying the convergence of turbo decoders without simulating the whole decoding process. We use the density evolution method in [24] to confirm our simulation.

We approximate the extrinsic information as a Gaussian variable whose mean is equal to half of the variance. In each iteration, we compute the average mean of the extrinsic information and then regenerate the extrinsic information as

an independent Gaussian variable. Thus, the dependence between the extrinsic information bits is wiped out. This is the main difference between density evolution and simulation. Since TCM is typically irregular, density evolution using the all-zero sequence may be biased. So we need to consider both 0-bit and 1-bit as inputs which could bring a negative mean according to the definition of extrinsic information in (29). We examine the mean of extrinsic information using tens of thousands of randomly generated bit sequences and make it always positive regardless of bit sequences by weighting the sign of the bit. Such a mean can be easily traced by two decoding trajectories in the density evolution chart, that is,

$$\mu_{L_e} = \overline{L_e(u_b)(2u_b - 1)}, \tag{32}$$

where overbar denotes the average. For UWB channels, we then average it over more than 2000 UWB channels.

Procedure of density evolution can be summarized as follows.

(1) Before the first iteration starts, all the extrinsic information is set to zero.
(2) We divide each decoding process into two halves—one half-iteration for TCM followed by another half-iteration for parity-check codes. For each half-iteration, we calculate the updated extrinsic information through decoding. Using tens of thousands of simulation, we get the mean of the densities of those updated extrinsic information using (32).
(3) Further, we assume the density to be Gaussian with the mean computed in (32) and the variance equal to twice the mean based on density symmetry condition [25]. Then, we regenerate the extrinsic information as an independent Gaussian variable for the next half-iteration.
(4) During each half-iteration, SNR is estimated as half of the mean of extrinsic information. SNR, before and after each half-iteration, can then be tracked in the density evolution chart as in this paper.

The EXIT chart (see Figure 8)is plotted as a combination of two charts, one is for $\mathrm{SNR1_{in}}$ and $\mathrm{SNR1_{out}}$ and the second is for $\mathrm{SNR2_{in}}$ and $\mathrm{SNR2_{out}}$. It shows input and output of extrinsic information (in terms of signal-to-noise ratio) for each decoder. Since the extrinsic information output of the first decoder is fed as the input for the second decoder, the combination of two charts easily demonstrates the convergent property of the code. For example, if two input-output curves are crossing, then the iterative decoder stops at the crossing point, which corresponds to a fixed nonzero error rate. Otherwise, the decoder produces extrinsic information with unbounded SNR, which corresponds to a zero error rate. The threshold is defined as the minimum value of signal-to-noise ratio that will generate two curves without a crossing point. Density evolution can be used to determine the threshold, which is the minimum SNR for the decoder to converge assuming infinite block length. In the density evolution chart, as long as the SNR is above the threshold, these two constituent transfer curves will never intersect, which means convergence in the limiting case. A detailed description of density evolution and EXIT chart can be found in [23, 25].

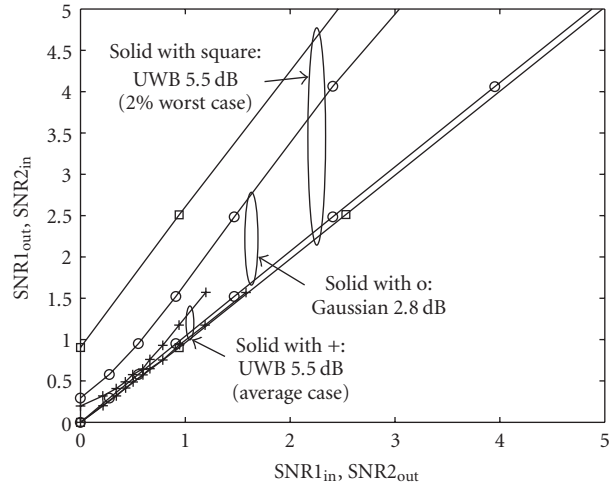

Figure 8: Density evolution for UWB/OFDM/16-QAM on AWGN and UWB channels.

In Figure 8, we show density evolution for OFDM systems using 16-QAM on Gaussian and UWB fading channels. For Gaussian channels, we find the threshold is 2.6 dB and show the EXIT chart for $E_b/N_0 = 2.8$ dB. On UWB channels, we find that if we take average over all 2000 channels, then EXIT chart shows the clear case of convergence (see curves with solid squares in Figure 8). However, if we run EXIT over each individual channel instance, then some channel instances require much larger SNRs to allow iterative decoding to converge to the correct codewords. For example, at $E_b/N_o = 5.5$ dB, about 2% of the channels are harder to converge (see curves with crosses in Figure 8). We call them "bad" channels. When E_b/N_o is small, the percentage of the worst channels increases significantly. For example, when $E_b/N_o = 4.5$ dB, about 20% of channels are bad. Good performance can only be achieved if the interleaver can fully randomize the extrinsic information over all channels. If the bits of a packet are interleaved over a number of channels containing significant amount of "bad" channels, then the performance will be much worse. This is the main reason that the packet error rate curve for UWB cannot drop sharply as those on AWGN channels.

Figure 9 presents the density evolution analysis for OFDM system using 64-QAM on Gaussian and UWB fading channels. For Gaussian channels, we find the threshold is 3.7 dB and show the EXIT chart for $E_b/N_o = 4.2$ dB. For UWB channels, when we set $E_b/N_o = 9.2$ dB, about 2% of the channels are bad.

5. NUMERICAL RESULTS

The performance of the coding/decoding scheme is evaluated and applied to the OFDM systems for UWB channels. A similar simulation has been done over AWGN channels

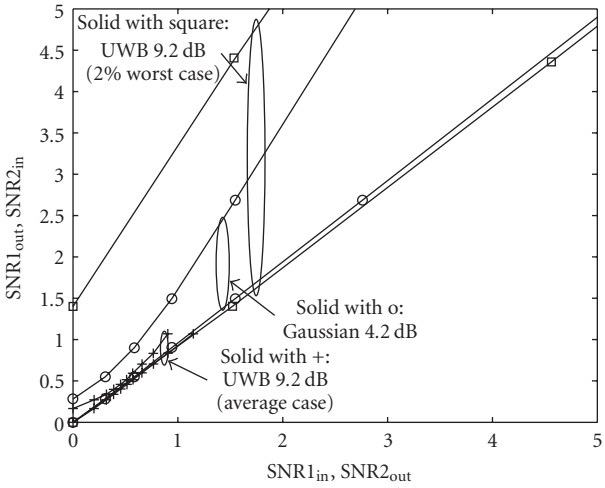

Figure 9: Density evolution for UWB/OFDM/64-QAM on AWGN and UWB channels.

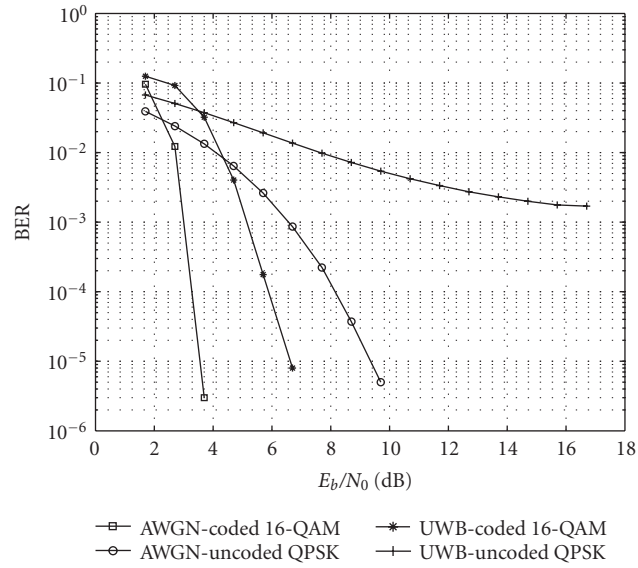

Figure 10: BER of OFDM/16-QAM over UWB and AWGN channel.

Table 1: COFDM system parameters.

Information data rate	640 Mbps / 1.2 Gbps
Constellation	16-QAM/64-QAM
16-state TCM code	(23,35,27)/(23,35,33,37,31)
FFT size	128
Data tones	100
System bandwidth	528 MHz
Subcarrier frequency spacing	4.125 MHz
IFFT/FFT period	242.42 ns
Cyclic prefix duration	60.61 ns
Gaurd interval duration	9.47 ns
Symbol interval	312.5 ns
Time-domain spreading	Yes
Multipath tolerance	60.6 ns
UWB channel model	AR model

for performance comparison. A 16-state TCM code with octal notation (23,35,27) is chosen with 16-QAM modulation and (23,35,33,37,31) for 64-QAM modulation. The resultant data rates are 640 Mbps and 1.2 Gbps, respectively. System-level simulations were performed to estimate the bit error rate (BER) and packet error rate (PER) performance. Table 1 shows a list of key COFDM parameters used in our simulations. The system is assumed to be perfectly synchronized. All simulation results are averaged over 2000 packets with a payload of 1 KB for 640 Mbps system and 2 KB for 1.2 Gbps system. There are 2000 different UWB channel realizations involved in the simulation.

Figure 10 shows the BER performance of the coded 16-QAM OFDM system and uncoded OFDM system in both UWB and AWGN channels as a function of E_b/N_0. Uncoded modulation scheme is QPSK in order to keep same system coding rate. For UWB channels, the line-of-sight (LOS) distance between the transmitter and receiver is 10 m. To measure BER at each point, we simulate up to 1.64×10^7 bits, which is 2000 packets $\times 41$ OFDM symbols/packet $\times 100$ QAM symbols/OFDM symbol $\times 2$ bits/QAM symbol. The coded OFDM curve shows a big performance improvement over uncoded OFDM, especially on UWB channels. Furthermore, a BER of 8×10^{-6} is obtained at $E_b/N_0 = 6.7$ dB. Figure 11 describes the PER performance of the 640 Mbps coded OFDM system and uncoded case over UWB and AWGN channels. The low PER of 0.036 is obtained at $E_b/N_0 = 6.7$ dB for coded OFDM over 10 m UWB channels.

The BER performance for 64-QAM coded OFDM system and 16-QAM uncoded OFDM system is illustrated in Figure 12. Again uncoded modulation scheme is lower than coded modulation scheme to keep the same system coding rate. There are 3.28×10^7 (2000 packets $\times 41$ OFDM symbols/packet $\times 100$ QAM symbols/OFDM symbol $\times 4$ bits/QAM symbol) random bits simulated to measure the BER. The LOS of the UWB channel distance is 10 m. The simulation results indicate a BER of 2.3×10^{-5} at $E_b/N_0 = 10.7$ dB for 1.2 Gbps coded OFDM system over UWB channels. Figure 13 presents the PER performance for the same situation, reporting a low PER of 0.011 at $E_b/N_0 = 10.7$ dB for 1.2 Gbps coded OFDM over UWB channels.

6. CONCLUSION

The proposed coding scheme utilizes a punctured parity-concatenated TCM encoder to function as a turbo TCM, which may have a big advantage in real-world implementation due to the savings of constituent encoder and

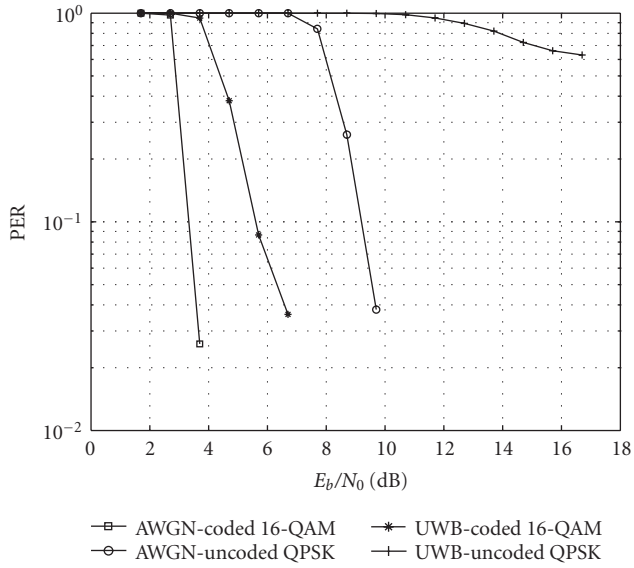

Figure 11: PER of OFDM/16-QAM over UWB and AWGN channel.

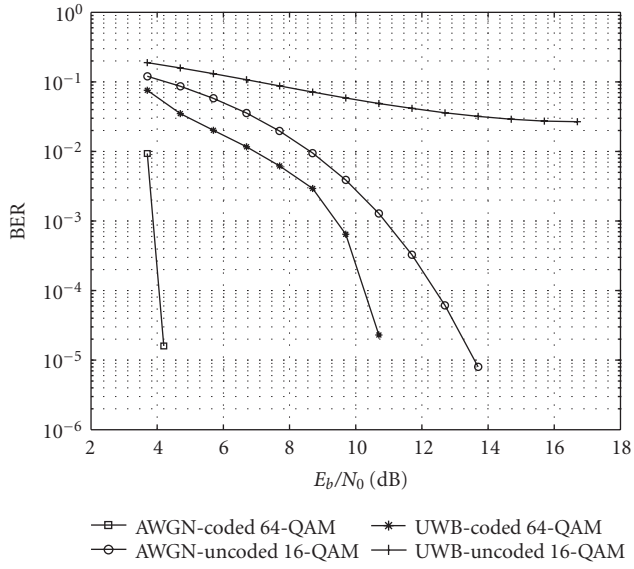

Figure 12: BER of OFDM/64-QAM over UWB and AWGN channel.

interleavers. The scheme can be applied to the OFDM system over UWB channels for higher spectral efficiency. We identify several essential requirements to achieve high rate such as frequency and time diversity, and multilevel error protection. The simulation results show that we can deliver data rates from 640 Mbps up to 1.2 Gbps to current UWB systems. The results are confirmed by density evolution. In the future, we will extend the TTCM to parity concatenated TCM (i.e., replacing repeater to single parity-check code) for rate change, and perform a more accurate analysis on its BER upper bound and possible error floor.

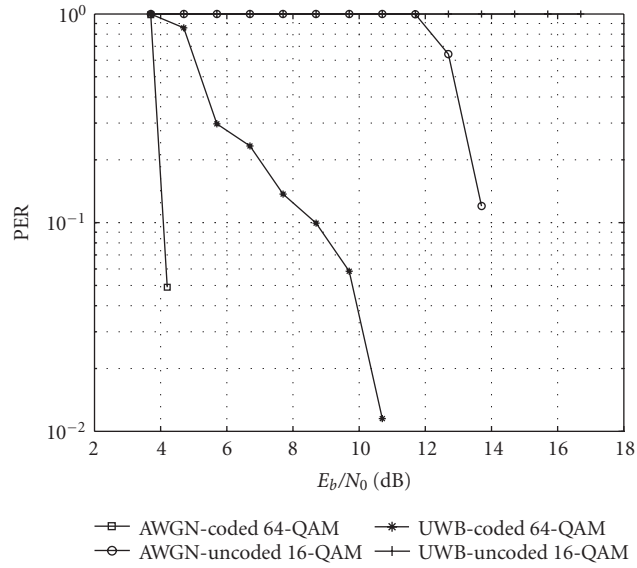

Figure 13: PER of OFDM/64-QAM over UWB and AWGN channel.

ACKNOWLEDGMENTS

This project was supported in part by the National Aeronautics and Space Administration through the University of Central Florida's Florida Space Grant Consortium. Part of this work was presented at ISIT 2005, Adelaide, Australia, September 2005.

REFERENCES

[1] M. Z. Win and R. A. Scholtz, "Characterization of ultra-wide bandwidth wireless indoor channels: a communication-theoretic view," *IEEE Journal on Selected Areas in Communications*, vol. 20, no. 9, pp. 1613–1627, 2002.

[2] A. F. Molisch, J. R. Foerster, and M. Pendergrass, "Channel models for ultrawideband personal area networks," *IEEE Wireless Communications*, vol. 10, no. 6, pp. 14–21, 2003.

[3] W. Turin, R. Jana, S. S. Ghassemzadeh, C. W. Rice, and T. Tarokh, "Autoregressive modeling of an indoor UWB channel," in *Proceedings of IEEE Conference on Ultra Wideband Systems and Technologies*, pp. 71–74, Baltimore, Md, USA, May 2002.

[4] L. J. Cimini Jr., "Analysis and simulation of a digital mobile channel using orthogonal frequency division multiplexing," *IEEE Transactions on Communications*, vol. 33, no. 7, pp. 665–675, 1985.

[5] A. Batra, et al., "Multi-band OFDM physical layer proposal for IEEE P802.15 task group 3a," IEEE P802.15-03/268r2, November 2003.

[6] B. L. Floch, M. Alard, and C. Berrou, "Coded orthogonal frequency division multiplex," *Proceedings of the IEEE*, vol. 83, no. 6, pp. 982–996, 1995.

[7] G. Ungerboeck, "Channel coding with multilevel/phase signalling," *IEEE Transactions on Information Theory*, vol. 28, no. 1, pp. 55–67, 1982.

[8] S. LeGoff, A. Glavieux, and C. Berrou, "Turbo-codes and high spectral efficiency modulation," in *Proceedings of IEEE*

International Conference on Communications (ICC '94), vol. 2, pp. 645–649, New Orleans, La, USA, May 1994.

[9] P. Robertson and T. Wörz, "Bandwidth-efficient turbo trellis-coded modulation using punctured component codes," *IEEE Journal on Selected Areas in Communications*, vol. 16, no. 2, pp. 206–218, 1998.

[10] S. Benedetto, D. Divsalar, G. Montorsi, and F. Pollara, "Parallel concatenated trellis coded modulation," in *Proceedings of IEEE International Conference on Communications (ICC '96)*, vol. 2, pp. 974–978, Dallas, Tex, USA, June 1996.

[11] G. D. Forney Jr., M. D. Trott, and S.-Y. Chung, "Sphere-bound-achieving coset codes and multilevel coset codes," *IEEE Transactions on Information Theory*, vol. 46, no. 3, pp. 820–850, 2000.

[12] Q. Wang, L. Wei, and R. A. Kennedy, "Iterative Viterbi decoding, trellis shaping, and multilevel structure for high-rate parity-concatenated TCM," *IEEE Transactions on Communications*, vol. 50, no. 1, pp. 48–55, 2002.

[13] Q. Wang and L. Wei, "Graph-based iterative decoding algorithms for parity-concatenated trellis codes," *IEEE Transactions on Information Theory*, vol. 47, no. 3, pp. 1062–1074, 2001.

[14] D. Divsalar, H. Jin, and R. J. McEliece, "Coding theorems for turbo-like codes," in *Proceedings of 36th Allerton Conference Communication, Control and Computing*, pp. 201–210, Monticello, Ill, USA, September 1998.

[15] A. Batra, J. Balakrishnan, G. R. Aiello, J. R. Foerster, and A. Dabak, "Design of a multiband OFDM system for realistic UWB channel environments," *IEEE Transactions on Microwave Theory and Techniques*, vol. 52, no. 9, pp. 2123–2138, 2004.

[16] M. Z. Win and R. A. Scholtz, "Impulse radio: how it works," *IEEE Communications Letters*, vol. 2, no. 2, pp. 36–38, 1998.

[17] A. Saleh and R. Valenzuela, "A statistical model for indoor multipath propagation," *IEEE Journal on Selected Areas in Communications*, vol. 5, no. 2, pp. 128–137, 1987.

[18] B. Muquet, Z. Wang, G. B. Giannakis, M. de Courville, and P. Duhamel, "Cyclic prefixing or zero padding for wireless multicarrier transmissions?" *IEEE Transactions on Communications*, vol. 50, no. 12, pp. 2136–2148, 2002.

[19] A. Scaglione, G. B. Giannakis, and S. Barbarossa, "Redundant filterbank precoders and equalizers —part I: unification and optimal designs and part II: blind channel estimation, synchronization, and direct equalization," *IEEE Transactions on Signal Processing*, vol. 47, no. 7, pp. 1988–2022, 1999.

[20] C. Berrou, A. Glavieux, and P. Thitimajshima, "Near shannon limit error-correcting coding and encoding: turbo-codes 1," in *Proceedings of IEEE International Conference on Communications (ICC '93)*, vol. 2, pp. 1064–1070, Geneva, Switzerland, May 1993.

[21] L. R. Bahl, J. Cocke, F. Jelinek, and J. Raviv, "Optimal decoding of linear codes for minimizing symbol error rate," *IEEE Transactions on Information Theory*, vol. 20, no. 2, pp. 284–287, 1974.

[22] D. Divsalar and F. Pollara, "On the design of turbo codes," JPL TDA Progress Report 42-123, Jet Propulsion Laboratory, Pasadena, Calif, USA, November 1995.

[23] S. ten Brink, "Convergence behavior of iteratively decoded parallel concatenated codes," *IEEE Transactions on Communications*, vol. 49, no. 10, pp. 1727–1737, 2001.

[24] D. Divsalar, S. Dolinar, and F. Pollara, "Serial turbo trellis coded modulation with rate-1 inner code," in *Proceedings of IEEE International Symposium on Information Theory (ISIT '00)*, p. 194, Sorrento, Italy, June 2000.

[25] D. Divsalar, S. Dolinar, and F. Pollara, "Iterative turbo decoder analysis based on density evolution," *IEEE Journal on Selected Areas in Communications*, vol. 19, no. 5, pp. 891–907, 2001.

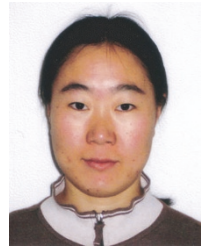

Yanxia Wang received the B.S. and M.S. degrees in electrical engineering from Wuhan Technical University of S&M, China, in 1993 and 1996, respectively, and an M.S. degree in electrical engineering from the School of Electrical Engineering and Computer Science, University of Central Florida, Orlando, USA, in 2001. She is now a Ph.D. candidate at the same university. From 1996 to 1999, she held a research and teaching position in Information Department of North China Electric Power University. Her general interests lie in the area of coding/decoding algorithm design and signal processing for wireless communications systems. Most recent research is in the area of turbo TCM coding/decoding, OFDM systems over ultra-wideband channel, and power-line channels.

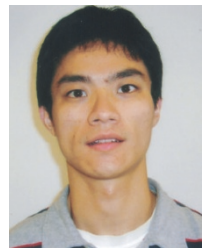

Libo Yang received the B.E. and M.E. degrees in electrical engineering, in 2000 and 2003, respectively, from Nanjing University of Posts and Telecommunications, China. He is currently working towards the Ph.D. degree in the School of Electrical Engineering and Computer Science at the University of Central Florida, Orlando, FLa, USA. His research interests are in the area of wireless communications and signal processing, currently working on error control codes design and analysis, and its application in ultra-wideband communications.

Lei Wei received the M.E. degree from the University of New South Wales, Sydney, Australia, in 1993, and the Ph.D. degree from the University of South Australia, Adelaide, Australia, in 1995, both in electrical engineering. From 1995 to 2000, he was a faculty member with the Department of Engineering, Australian National University, Canberra, Australia. During 2000–2001, he was with the Telecommunications Information Technology Research Institute (TITR), University of Wollongong, Wollongong, Australia, as an Associate Professor. He is now with the Department of Electrical and Computer Engineering, University of Central Florida, Orlando, as an Associate Professor. His current research interests include iterative decoding, reliability study for ad hoc networks, digital modulation, UWB, spread-spectrum multiple access with applications to mobile communications, and biologically inspired signal processing. He was the Founder and Chair of the Australian Information Theory Chapter, 1999, and a Member of the Organization Committee for the International Symposium on Information Theory and Its Applications (ISITA 2000). He was a Cochair of the IEEE Information Theory Workshop, Cairns, Australia, September 2001, a Member of the Technical Program Committee for the IEEE International Conference on Communications (ICC 2002), and an Associate Editor for IEEE Transactions on Communications in the area of wireless communications from 1999 to 2003.